Sensors & Diagnostics

PAPER

View Article Online
View Journal | View Issue

Check for updates

Cite this: *Sens. Diagn.*, 2023, **2**, 1605

Platinum nanozyme-mediated temperature sensor for sensitive photothermal immunoassay of YKL-40 under near-infrared light

Shaoyang Yu,†[a] Qiaohong Ke,†[a] Fan Cai,†[b] Sisi Gong,[a] Rongfu Huang[a] and Chunmei Fan *[a]

Received 21st August 2023,
Accepted 29th September 2023

DOI: 10.1039/d3sd00222e

rsc.li/sensors

This work reports on the proof-of-concept of an innovative photothermal immunosensing platform for the sensitive screening of YKL-40 in biological fluids by coupling near-infrared light (NIR)-excited platinum nanoparticles (PtNPs) with a handheld digital thermometer. First, a sandwiched immunoreaction was performed on a monoclonal rabbit anti-human YKL-40 capture antibody-coated microplate using PtNP-labeled anti-YKL-40 secondary antibody. After the formation of the sandwiched immunocomplex, the carried PtNP caused the photothermal conversion under 808 nm laser irradiation relative to the 3,3′,5,5′-tetramethylbenzidine (TMB)–H_2O_2 system, thereby, resulting in an increase in the temperature of the detection solution. Under optimum conditions, the PtNP-based photothermal immunoassay exhibited a linear relationship within a dynamic range of 0.03–100 ng mL^{-1} at a low limit of detection of 0.014 ng mL^{-1} YKL-40. High specificity, good reproducibility, and long-term stability were achieved with this system. In addition, the accuracy of this method was evaluated for the analysis of human serum samples, giving well-matched results compared with the human YKL-40 enzyme-linked immunosorbent assay.

Open Access Article. Published on 04 October 2023. Downloaded on 5/23/2026 9:15:54 AM.
This article is licensed under a Creative Commons Attribution-NonCommercial 3.0 Unported Licence.

Introduction

YKL-40 (coded as gene chitinase-3-like protein 1, a secreted glycoprotein) is classified as a member of the glycoside hydrolase family 18.[1] It is also a carbohydrate-binding lectin with a preference for chitin that plays an important role in tissue remodeling and cell response to changes in the environment.[2,3] In the physiological condition, YKL-40 is expressed by different cell types, including macrophages, chondrocytes, synoviocytes, and neutrophils.[4] It is known that YKL-40 is essential for tissue macrophage differentiation from monocytes and vascular cell activation. Typically, increased YKL-40 levels in the blood are associated with the progression of multiple diseases and cancers, such as gastric cancer, colon cancer, and glioma cancer.[5] Interestingly, YKL-40 secreted from macrophages can induce cell migration and invasion of colon, gastric, and breast cancers. Therefore, sensitive and specific detection of YKL-40 in biological fluids is of great interest for clinical diagnostics.

Recently, different methods and strategies have been reported and developed for the detection of YKL-40, including enzyme-linked immunosorbent assay (ELISA), electrochemical method, and optical assays.[6,7] Schmalenberg *et al.* developed a magnetic bead fluorescent immunoassay for the rapid detection of the inflammation marker YKL-40.[8] The Chaocharoen group designed a label-free electrochemical immunosensor for the voltammetric detection of human chitinase-3-like protein 1 by matching the antibody-modified gold electrode.[9] Ceuninck *et al.* fabricated an enzyme-linked immunoassay for the quantification of YKL-40 using hen egg yolk antibodies.[10] Despite some advances in this field, there is still a need to explore sensitive immunosensing systems to simplify the operation process. Recent studies have mainly focused on the development and preparation of immunoassays with the aim of manufacturing portable and affordable diagnostic devices.[11,12] Point-of-care testing (POCT) and medical testing at the site of patient care bring the test conveniently and immediately to the patient.[13] Yu *et al.* prepared a paper electrode-based flexible pressure sensor for the point-of-care immunoassay using a digital multimeter.[14] Zeng *et al.* constructed a smartphone-based electrochemical immunoassay for the point-of-care detection of SARS-CoV-2 nucleocapsid protein.[15] Our motivation for this study was to explore an affordable point-of-care immunoassay for the sensitive monitoring of YKL-40.

The digital thermometer is currently one of the most widely used temperature sensors because of its portable size, easy operation, low cost, and reliable quantitative results.[16] Lu *et al.* proposed a dual-mode photoelectrochemical and

[a] *Clinical Laboratory Center, The Second Affiliated Hospital of Fujian Medical University, Quanzhou 362000, P. R. China. E-mail: fanchunmei9575@163.com*
[b] *College of Life Sciences, Fujian Normal University, Fuzhou 350117, P. R. China*
† These authors equally contributed to this work.

© 2023 The Author(s). Published by the Royal Society of Chemistry

Open Access Article. Published on 04 October 2023. Downloaded on 5/23/2026 9:15:54 AM.
This article is licensed under a Creative Commons Attribution-NonCommercial 3.0 Unported Licence.

photothermal immunoassay coupled with an Ag/MoO_3–Pd-mediated gasochromic reaction.[17] Yu *et al.* innovatively developed a flexible and high-throughput photothermal biosensor for rapid screening of acute myocardial infarction using thermochromic paper-based image analysis.[18] For the successful development of photothermal immunoassay, the design of a photo-heat conversion system is very important. Routine approaches generally involve an enzyme label or a nano label.[19] Enzyme-based immunoassays are susceptible to interference and changes in assay conditions during the signal generation stage.[20] In contrast, the emergence of nanotechnology has opened a new horizon for the use of nano labels for photothermal immunoassays. To the best of our knowledge, there has been no report focusing on nanozyme-based photothermal immunoassay for YKL-40 until now.

As is well-known, nanometer-sized platinum nanoparticles can exhibit highly catalytic activity for the reduction of hydrogen peroxide (H_2O_2).[21–24] Actually, platinum nanozyme can not only catalyze the oxidation of H_2O_2 with the peroxidase-like activity,[20] but also display the laccase-like activity and antioxidant capacity in different matrices.[25–27] In this work, substrate H_2O_2 was only used as a model for the development of platinum nanozyme-based photothermal immunoassay. Under near-infrared (NIR) light irradiation, the photo-heat conversion can be readily carried out using platinum nanoparticles (PtNP) relative to the 3,3′,5,5′-tetramethylbenzidine (TMB)–H_2O_2 system.[28] PtNP can be used as peroxidase-like mimic to oxidize TMB into the photothermal product, oxidized TMB (ox-TMB) during the process, thus increasing the temperature of the solution. With the PtNP–TMB–H_2O_2 system, we designed an innovative photothermal immunoassay for the portable detection of YKL-40 by using the PtNP-labeled detection antibody on the capture antibody-coated microplate with a sandwiched reaction mode. By monitoring the temperature change using a handheld digital thermometer, we quantitatively evaluated the concentration of target YKL-40 in the sample (Scheme 1).

Experimental section

Materials and reagents

Human YKL-40 ELISA kit (one-wash 90 min protocol, sensitivity: 3.9 pg mL^{-1}, range: 23.44–1500 pg mL^{-1}), monoclonal rabbit anti-human YKL-40 antibody (mAb_1, clone: EPR19078-1571), and monoclonal rabbit anti-human YKL-40 antibody (mAb_2, clone: EPR27396-56) were purchased from Abcam (Shanghai, China). Platinum nanoparticles (PtNPs; pure, 20 nm in water at 500 mg L^{-1} surfactant and reactant-free, stabilized with <0.01 mM of citrate to enhance the stability of platinum nanoparticles and the conjugated capacity with the antibodies) were obtained from Aladdin (Shanghai, China). All high-binding polystyrene 96-well microtiter plates were obtained from Greiner (Ref. 655061, Greiner, Frickenhausen, Germany). Bovine serum albumin (BSA, 96–99%) and 3,3′,5,5′-tetramethylbenzidine (TMB) were purchased from Sinopharm Chem. Re. Co., Ltd. (Shanghai, China). All other reagents were of analytical grade and were used without further purification. Ultrapure water obtained using a Millipore water purification system (18.2 MΩ, Milli-Q, Millipore) was used in all runs.

A pH 9.6 coating buffer (1.59 g Na_2CO_3, 2.93 g $NaHCO_3$, and 0.2 g NaN_3) and a pH 7.4 phosphate-buffered saline (PBS, 0.01 M) (2.9 g $Na_2HPO_4{\cdot}12H_2O$, 0.24 g KH_2PO_4, 0.2 g KCl, and 8.0 g NaCl) were prepared by adding the corresponding chemicals into 1000 mL distilled water. The blocking buffer and washing buffer were obtained by adding 1.0% BSA (w/v) and 0.05% Tween 20 (v/v) in PBS, respectively.

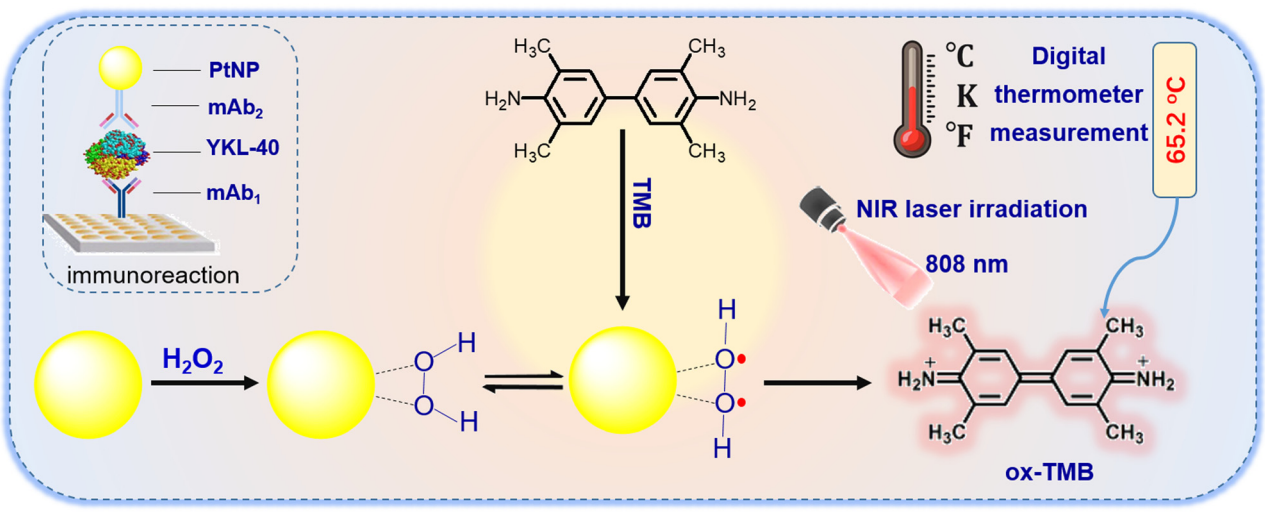

Scheme 1 Schematic illustration of the PtNP-based photothermal immunoassay to target YKL-40 on monoclonal rabbit anti-human YKL-40 capture antibody (mAb_1)-coated microplate using monoclonal rabbit anti-human YKL-40 secondary antibody (mAb_1)-labeled platinum nanoparticle (PtNP) with a sandwich-type immunoreaction mode relative to the 3,3′,5,5′-tetramethylbenzidine (TMB)–H_2O_2 system under 808 nm near-infrared (NIR) laser irradiation.

© 2023 The Author(s). Published by the Royal Society of Chemistry

Open Access Article. Published on 04 October 2023. Downloaded on 5/23/2026 9:15:54 AM. This article is licensed under a Creative Commons Attribution-NonCommercial 3.0 Unported Licence.

Labelling of PtNPs with mAb_2 antibodies

Prior to the experiment, 5.0 mL of 20 nm platinum colloids (PtNPs, $C_{[Pt]}$ = 24 μM) was adjusted to pH 9.0–9.5 by directly using 0.1 M Na_2CO_3 aqueous solution. Thereafter, 500 μL of mAb_2 antibodies (1.0 mg mL^{-1}) in PBS (pH 7.4, 0.01 M) were added to the platinum colloid. After gently shaking for 5 min, the mixture was transferred to the refrigerator at 4 °C for further reaction (overnight). During this process, mAb_2 antibodies were covalently bound to PtNPs *via* the dative binding between PtNPs and free-SH groups of the antibody.[29] Following that, the mixture was then centrifuged (13 000*g*) for 25 min at room temperature. The mAb_2-functionalized platinum nanoparticles (designated as mAb_2-PtNPs) were re-suspended in 1.0 mL of 2.0 mM sodium carbonate solution containing 1.0 wt% BSA and 0.1% sodium azide, pH 7.4, and stored at 4 °C until use.

Preparation of mAb_1 capture antibody-coated microplate

A high-binding polystyrene 96-well microplates (Ref. 655061, Greiner, Frickenhausen, Germany) were coated overnight at 4 °C with 50 μL per well of mAb_1 antibody at a concentration of 10 μg mL^{-1} in 0.05 M sodium carbonate buffer (pH 9.6). The microplates were covered with an adhesive plastic plate sealing film to prevent evaporation. On the following day, the plates were washed three times with the washing buffer and then incubated with 300 μL per well of blocking buffer for 1 h at 37 °C with shaking. The plates were washed as before for use.

Immunoreaction protocol and photothermal measurements

Initially, 50 μL of YKL-40 standards or samples with various concentrations in PBS (pH 7.4, 10 mM) were added to the microplates and incubated for 1 h at 37 °C under shaking. After washing, 50 μL of the above-prepared mAb_2-PtNP suspension was added to the well and incubated for 1 h at 37 °C with shaking. After washing with the washing buffer, 100 μL of the substrate solution containing 7.63 M H_2O_2 and 0.921 mM TMB in PBS (10 mM, pH 7.4) was added to each well. The plates were then shaken for 1.0 min on a plate shaker for the photothermal measurement. The temperature sensor was inserted into the microplate (close to the bottom of the well) and the temperature of the detection solution was determined after coupling it with the photo-heat conversion system on a portable VICTOR 86 digital thermometer using an 808 nm adjustable laser irradiation (2.5 W cm^{-2}). To avoid possible errors resulting from the different-batch introduction of the digital thermometer, the signal for each well was recorded as the irradiation from 30 s onwards (after the introduction of the thermometer) until the equilibrium was reached at ~8 min (optimized). The control tests with normal (negative) samples and the evaluations for human serum specimens were performed accordingly. The collected temperature relative to the target YKL-40 concentration was recorded as the signal of the photothermal immunoassay. All the determinations were made at least in duplicate. All the measurements were carried out at room temperature (25 ± 1.0 °C) unless mentioned otherwise. The sigmoidal curves were calculated by mathematically fitting the experimental points using Rodbard's four-parameter function with Origin 6.0 software. Graphs were plotted in the form of absorbance against the logarithm of YKL-40 concentration.

Results and discussion

Characterization of mAb_2-PtNPs

In this work, the photo-heat conversion system was prepared using the as-synthesized platinum nanoparticles under near-infrared laser irradiation relative to the TMB–H_2O_2 system. To realize our design, the successful preparation of platinum nanoparticles and mAb_2-PtNPs was very crucial prior to the measurement. Firstly, we used transmission electron microscopy (TEM, H-7700, Hitachi Instruments, Tokyo, Japan) to characterize the platinum nanoparticles. As shown in Fig. 1A, the average size of the as-purchased platinum nanoparticles was 20 nm in diameter. Such nanoparticles could provide a relatively large surface area for the labelling of mAb_2 antibodies. From a statistical point of view, we could roughly estimate that one solid platinum nanoparticle with 20 nm in diameter could simultaneously label 64 mAb_2 antibodies at most. The calculation was performed on the basis of the assumption of spherical surface area ($S_{NP} = 4\pi r_{NP}^2$) divided by the area of antibody's radius-based circle ($S_{Ab} = \pi r_{Ab}^2$), where r_{NP} stands for the radius of PtNP and r_{Ab} stands for the radius of antibody (~5.0 nm in diameter).

To further investigate the successful labelling of mAb_2-PtNP, dynamic light scattering (DLS; Zetasizer Nano S90, Malvern Instruments, Malvern, UK) was utilized to monitor the sizes of platinum nanoparticles before and after labelling with mAb_2 antibodies. As indicated in Fig. 1B, platinum nanoparticles alone gave an average hydrodynamic size of 21.2 ± 1.3 nm (bottom panel). Favorably, the average hydrodynamic size of mAb_2-PtNPs increased to 33.6 ± 2.7 nm (top panel). The increased size mainly originated from the labeled mAb_2 antibodies on the surface of the platinum nanoparticles. These results indicated that mAb_2 antibodies could be labeled onto the platinum nanoparticles.

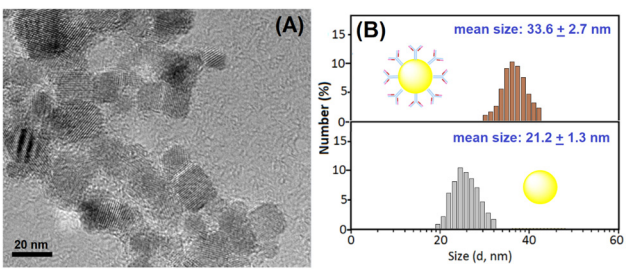

Fig. 1 (A) Transmission electron microscopic (TEM) image of platinum nanoparticles. (B) Dynamic light scattering (DLS) data of (bottom) PtNPs and (top) mAb_2-PtNPs.

Open Access Article. Published on 04 October 2023. Downloaded on 5/23/2026 9:15:54 AM. This article is licensed under a Creative Commons Attribution-NonCommercial 3.0 Unported Licence.

Evaluation of feasibility

Using the as-prepared mAb_2-PtNPs, we studied the feasibility of the developed photothermal immunoassay for the detection of target YKL-40 on mAb_1-coated microplate. The temperature was measured after the sandwiched immunoreaction (*i.e.*, mAb_1-YKL-40-mAb_2-PtNP) relative to TMB–H_2O_2 system under 808 nm NIR irradiation. 1.0 ng mL^{-1} YKL-40 was used as an example in this case. As seen from Fig. 2A, the temperature increased from 25 °C to about 44.9 °C with the increasing irradiation time in the presence of 1.0 ng mL^{-1} YKL-40. The steady-state temperature could be acquired after ~8.0 min. As control tests, a series of experiments were carried out relative to the different systems (Fig. 2B). Almost no temperature changes relative to room temperature were observed for the mAb_1-coated microplate before (column 'a') and after (column 'b') the reaction with 1.0 ng mL^{-1} YKL-40 in the TMB–H_2O_2 system under 808 nm NIR irradiation. After the reaction of mAb_1-YKL-40 with mAb_2-PtNP, the temperature shift was largely increased relative to the TMB–H_2O_2 system under 808 nm NIR irradiation (column 'c'). For comparison, mAb_2 antibodies without the labeled PtNP were directly used to react with mAb_1-YKL-40. As indicated in column 'd', the temperature was almost the same as room temperature. These results revealed that the increase in the temperature of the TMB–H_2O_2 solution was derived from the labelled PtNPs under the NIR irradiation.

Typically, the synthesized PtNPs could exhibit peroxidase-like activity for the development of colorimetric immunoassays relative to the TMB–H_2O_2 system.[30,31] That is to say, it is not necessary to trigger the peroxidase-like activity of PtNPs by the NIR irradiation. To further investigate the role of NIR irradiation in our system, 1.0 ng mL^{-1} YKL-40 was detected by the developed photothermal immunoassay with and without NIR irradiation. As seen from columns 'c' and 'e', the temperature shift under the NIR irradiation was bigger than that without the NIR irradiation. In this case, the NIR irradiation could amplify the detectable signal of the photothermal immunoassay. Furthermore, we also studied the roles of TMB and H_2O_2 in this work. The formed sandwiched immunocomplexes (*i.e.*, mAb_1-YKL-40-mAb_2-PtNP) were monitored with and without TMB or H_2O_2. Results indicated that the temperatures were not changing in the absence of TMB (column 'f') and H_2O_2 (column 'g') under 808 nm NIR irradiation, suggesting that the temperature change mainly originated from the TMB–H_2O_2 solution by the labelled PtNP. In addition, the mAb_1-coated microplate was directly used for the incubation of mAb_2-PtNPs in the absence of YKL-40 (*i.e.*, 0 ng mL^{-1}). Curve 'h' in Fig. 2B gives the experimental results. Obviously, the temperature was close to room temperature (25 °C), suggesting that mAb_2-PtNPs were not nonspecifically adsorbed on the mAb_1-coated microplate and the temperature change was derived from the introduction of PtNPs. On the basis of the above results, we made a conclusion that our designed system could be preliminarily applied for the detection of YKL-40.

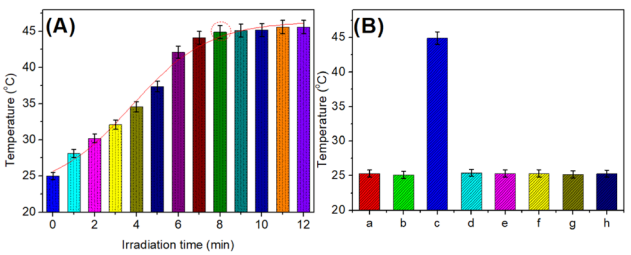

Fig. 2 (A) Temperature responses of photothermal immunoassay with increasing irradiation time toward 1.0 ng mL^{-1} YKL-40 under 808 nm NIR light irradiation in the TMB–H_2O_2 system; (B) temperature responses of (a) mAb_1 + TMB + H_2O_2 + NIR, (b) mAb_1 + 1.0 ng mL^{-1} YKL + TMB + H_2O_2 + NIR, (c) mAb_1 + 1.0 ng mL^{-1} YKL + mAb_2-PtNP + TMB + H_2O_2 + NIR, (d) mAb_1 + 1.0 ng mL^{-1} YKL + mAb_2 + TMB + H_2O_2 + NIR, (e) mAb_1 + 1.0 ng mL^{-1} YKL + mAb_2-PtNP + TMB + H_2O_2, (f) mAb_1 + 1.0 ng mL^{-1} YKL + mAb_2-PtNP + H_2O_2 + NIR, (g) mAb_1 + 1.0 ng mL^{-1} YKL + mAb_2-PtNP + H_2O_2 + NIR, and (h) mAb_1 + 0 ng mL^{-1} YKL + mAb_2-PtNP + TMB + H_2O_2 + NIR.

Analytical performance of PtNP-based photothermal immunoassay

With the as-prepared mAb_2-PtNPs, YKL-40 standards with various concentrations were measured using a handheld digital thermometer using our designed photothermal immunoassay. The assay was carried out as follows: $\Delta T = T_{max} - T_{surr}$, where T_{max} and T_{surr} represent the steady-state temperature and the surrounding temperature of the detection solution, respectively. The surrounding temperature referred to as room temperature, 25 °C. As indicated in Fig. 3A, the temperature increased with the increment of the YKL-40 level in the sample. A sigmoidal relationship between the temperature change and the logarithm of YKL-40 concentrations was obtained with a dynamic range of 0.001–100 ng mL^{-1}. Within the ranges of low-concentration YKL-40 (from 0.001 to 0.03 ng mL^{-1}) or high concentrations (from 100 to 1000 ng mL^{-1}), the change in the temperature was not obvious. However, a good linear relationship between temperature and the decimal logarithm of YKL-40 concentration was acquired within the dynamic ranges from 0.03 to 100 ng mL^{-1}. The regression equation was ΔT (°C) = 19.35 + 9.94 × log $C_{[YKL\text{-}40]}$ (ng mL^{-1}, r = 0.9916, n = 9). The limit of detection (LOD) was calculated to be 0.014 ng mL^{-1} at a signal-to-noise ratio of 3σ (where σ is the standard deviation of the blank, n = 11). The LOD was calculated as follows, initially, we assayed the temperature change toward the blank sample 11 times. Thereafter, the standard deviation for 11 times was calculated to be ~0.317. Finally, the 3 × SD was substituted to the above-mentioned regression equation to calculate the corresponding LOD. Furthermore, the LOD of PtNP-based photothermal immunoassay was comparable with those of commercial human YKL-40 ELISA kits (*e.g.*, 8.15 pg mL^{-1}

© 2023 The Author(s). Published by the Royal Society of Chemistry

Open Access Article. Published on 04 October 2023. Downloaded on 5/23/2026 9:15:54 AM.
This article is licensed under a Creative Commons Attribution-NonCommercial 3.0 Unported Licence.

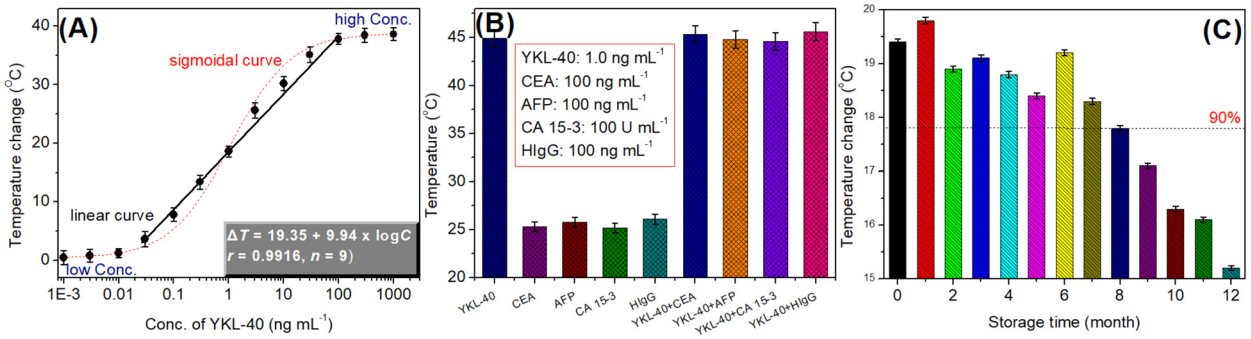

Fig. 3 (A) Calibration curve of PtNP-based photothermal immunoassay toward different YKL-40 levels under 808 nm NIR light irradiation for 8 min. (B) The specificity of the assay under 808 nm NIR light irradiation against YKL-40, CEA, AFP, CA 15-3, and HIgG. (C) The storage stability of mAb_1-coated microplates and mAb_2-PtNP at 4 °C.

from R & D Systems on cat# DC3L10; 3.9 pg mL^{-1} from Abcam on cat# ab255719). Compared with the optical readout, the developed photothermal immunoassay could be carried out by using a portable handheld thermometer (not using an expensive instrumentation). Unfavorably, one disadvantage of our system was that it was implemented under an 808 nm NIR irradiation.

To monitor the specificity of our method, other cancer biomarkers, *e.g.*, carcinoembryonic antigen (CEA), cancer antigen 15-3 (CA 15-3), alpha-fetoprotein (AFP), and human IgG (HIgG) were monitored by using PtNP-based photothermal immunoassay. As seen from Fig. 3B, the shifts in the temperatures on our system were close to zero toward non-targets including CEA, CA 15-3, AFP, and HIgG. However, an obvious increase in the temperature was achieved in the presence of target YKL-40. Moreover, the co-existence of non-targets with YKL-40 did not cause significant changes in the temperature. These results revealed that PtNP-based photothermal immunoassay had good selectivity and specificity.

Next, we investigated the reproducibility of PtNP-based photothermal immunoassay with the different batches of mAb_2-PtNPs and mAb_1-coated microplates, respectively. As seen from Table 1, all the relative standard deviations (RSDs) were less than 15%. However, the RSDs of using different-batch products were slightly more than those using the same-batch products. So, the reproducibility of PtNP-based photothermal immunoassay was acceptable.

The storage stability of mAb_2-PtNPs and mAb_1-coated microplates was investigated at 4 °C. The evaluation was determined by assaying 1.0 ng mL^{-1} YKL-40 at different storage times. As shown in Fig. 3C, the detectable signals could preserve >90% of the initial temperature after 8 months. Thus, the stability of mAb_2-PtNPs and mAb_1-coated microplates was satisfactory.

Analysis of human serum samples and method accuracy

15 human serum specimens including target YKL-40 were collected from our hospital, and measurements were performed using the PtNP-based photothermal immunoassay. Firstly, these serum samples were analyzed using the commercial human PSA ELISA kit. The high-concentration serum samples were diluted with PBS (10 mM, pH 7.4) for the measurement. These results are listed in Table 2. Statistical comparison of experimental results of photothermal immunoassay with those of human YKL-40 ELISA kit was performed by using a *t*-test for comparison of means preceded by the application of an *F*-test. The *t* statistics for each sample were calculated by using an independent two-sample *t*-test with equal sample sizes and equal variance as follows:

$$t = \frac{\overline{X}_1 - \overline{X}_2}{S_{X_1X_2} \cdot \sqrt{\frac{2}{n}}} \quad (1)$$

where

$$S_{X_1X_2} = \sqrt{\frac{1}{2}\left(S_{X_1}{}^2 + S_{X_2}{}^2\right)} \quad (2)$$

Here $\bar{X}_1$ and $S_{\bar{X}}$ are the means of each YKL-40 sample estimated with the photothermal immunoassay and the

Table 1 The reproducibility of PtNP-based photothermal immunoassay with the different-batch mAb_2-PtNPs and mAb_1-coated microplates toward 0.1, 10, and 50 ng mL^{-1} YKL-40 standards (unit: ng mL^{-1})

Sample	The same batch (time, conc./ng mL^{-1})			RSD	Different batches (time, conc./ng mL^{-1})			RSD
ng mL^{-1}	1	2	3	(%)	1	2	3	(%)
0.1	0.098	0.093	0.11	8.71	0.14	0.11	0.12	12.4
10	9.5	10.3	9.8	4.09	9.1	11.2	10.4	10.4
50	53.1	48.7	49.2	4.79	48.1	54.2	51.3	5.96

Open Access Article. Published on 04 October 2023. Downloaded on 5/23/2026 9:15:54 AM.
This article is licensed under a Creative Commons Attribution-NonCommercial 3.0 Unported Licence.

Table 2 Comparison of the assay results for human serum samples between PtNP-based photothermal immunoassay and commercial human YKL-40 ELISA kit

Sample no.[a]	Method; concentration (mean ± SD, n = 3, ng mL^{-1})		RSD[b] (%)	t_{exp}
	Photothermal immunoassay	YKL-40 ELISA kit		
1	46 ± 3	48 ± 2	4.2	1.37
2	32 ± 2	33 ± 1	2.2	0.68
3	78 ± 4	82 ± 7	3.4	0.83
4	21 ± 2	20 ± 2	3.7	0.79
5	13 ± 1	14 ± 1	5.7	1.12
6	90 ± 5	91 ± 7	0.8	0.19
7	46 ± 4	44 ± 3	2.2	0.49
8	87 ± 8	86 ± 4	1.3	0.32
9	76 ± 7	78 ± 6	2.1	0.44
10	33 ± 3	30 ± 1	4.7	1.25
11	8 ± 1	8 ± 0.6	6.2	1.32
12	24 ± 1	22 ± 2	5.3	1.44
13	3 ± 0.2	3 ± 0.1	2.2	0.77
14	0.3 ± 0.02	0.3 ± 0.01	7.0	2.32
15	0.03 ± 0.001	0.03 ± 0.002	9.1	3.09

[a] Samples #13–15 were initially achieved by diluting sample #10 to 10×, 100×, and 1000× with pH 7.4 PBS (10 mM), and then determined through these two methods. [b] RSDs were calculated on the basis of the mean values obtained by these two methods per sample.

standard error of the mean, respectively (1 = group one, 2 = group two), and n stands for the assay times for each sample. No significant differences were encountered between the two methods at the 0.05 significance level (Table 2) because all t_{exp} values were less than 4.30 ($t_{crit[0.05,2]}$ = 4.30) (t_{exp}: experimental value; t_{crit}: critical value), indicating a good method accuracy between the two methods.

Conclusions

In summary, we successfully designed an innovative photothermal immunoassay by using a portable handheld digital thermometer as the readout. Experimental results indicated that the developed photothermal immunoassay could exhibit high sensitivity, good reproducibility, specificity, long-term storage stability, and satisfactory method accuracy. Compared with our previous works on the immunoassays,[32–34] the highlights of our system could be simply summarized as follows: (i) the assay does not require expensive instrumentations and complex operation, and (ii) our strategy does not require the introduction of natural enzymes. Although our system mainly focuses on the detection of the target YKL-40, it is easy to extend it for the detection of other cancer biomarkers by changing the corresponding antibodies, thereby representing a universal method.

Compliance with ethical standards

All experiments were performed in accordance with the Guidelines of Fujian Medical University, and approved by the ethics committee at Fuzhou Medical University, China. Informed consent was obtained from human participants in this study.

Author contributions

Shaoyang Yu: conceptualization, methodology, investigation, writing – original draft. Qiaohong Ke: conceptualization, visualization, investigation, writing – original draft. Fan Cai: conceptualization, visualization, investigation, writing – original draft. Sisi Gong: resources, software, data curation. Rongfu Huang: investigation, validation, formal analysis, writing – original draft. Chunmei Fan: funding acquisition, supervision, writing – review and editing.

Conflicts of interest

There are no conflicts to declare.

Acknowledgements

Authors acknowledge the financial support from the Natural Science Foundation of Fujian Province (grant no.: 2020J01214).

References

1 B. Cui, Y. Chen, F. Luo, S. Lin, H. Liu, Y. Huang, Y. Zhou, Y. Tian, G. Yin and Q. Xie, *J. Clin. Lab. Anal.*, 2022, **36**, e24605.
2 Y. Jin, J. Song, F. Xu, D. Zhang, J. He, J. Zheng, Y. Zhang, J. Li, Y. Guo, M. Xu, X. Yu, Y. Liu, M. Liu and J. Yan, *Sleep Breath.*, 2022, **26**, 1011–1022.
3 D. O'Day and R. Huber, *BMC Neurosci.*, 2022, **23**, 10.
4 Z. Wang, S. Wang, Z. Jia, Y. Hu, D. Cao, M. Yang, L. Liu, L. Gao, S. Qiu, W. Yan, Y. Li, J. Luo, Y. Geng, J. Zhang, Z. Li, X. Wang, M. Li, R. Shao and Y. Liu, *Cancer Lett.*, 2023, **563**, 216184.
5 N. Dai, B. Jones and M. Husain, *Brain Sci.*, 2022, **12**, 1513.
6 S. Xu, X. Hu, J. Wang, Q. Xu, Z. Han, H. Zhou and M. Gao, *Clin. Chim. Acta*, 2023, **547**, 117443.

© 2023 The Author(s). Published by the Royal Society of Chemistry

Open Access Article. Published on 04 October 2023. Downloaded on 5/23/2026 9:15:54 AM.
This article is licensed under a Creative Commons Attribution-NonCommercial 3.0 Unported Licence.

7 J. Pereira, V. Fernandes, T. Alfaro, S. Freitas and C. Cordeiro, *Life*, 2023, **13**, 565.
8 M. Schmalenberg, C. Beaudoin, L. Bulst, D. Steubl and P. Luppa, *J. Immunol. Methods*, 2015, **427**, 36–41.
9 W. Chaocharoen, W. Suginta, W. Limbut, A. Ranok, A. Numnuam, P. Khunkaewla, P. Kanatharana, P. Thavarungkul and A. Schulte, *Bioelectrochemistry*, 2015, **101**, 106–113.
10 F. Ceuninck, P. Pastoureau, S. Agnellet, J. Bonnet and P. Vanhoutte, *J. Immunol. Methods*, 2002, **252**, 153–161.
11 H. Yuan, P. Chen, C. Wan, Y. Li and B. Liu, *TrAC, Trends Anal. Chem.*, 2022, **157**, 116814.
12 D. Kinnamon, J. Heggestad, J. Liu and A. Chilkoti, *Annu. Rev. Anal. Chem.*, 2022, **15**, 123–149.
13 M. Puiu, C. Nativi and C. Bala, *TrAC, Trends Anal. Chem.*, 2023, **160**, 116981.
14 Z. Yu, Y. Tang, G. Cai, R. Ren and D. Tang, *Anal. Chem.*, 2019, **91**, 1222–1226.
15 R. Zeng, M. Qiu, Q. Wan, Z. Huang, X. Liu, D. Tang and D. Knopp, *Anal. Chem.*, 2022, **94**, 15155–15161.
16 L. Easterwood and N. Cohen, *J. Equine Vet. Sci.*, 2023, **123**, 104243.
17 L. Lu, X. Hu, R. Zeng, Q. Lin, X. Huang, Q. Wei, D. Tang and D. Knopp, *Biosens. Bioelectron.*, 2023, **230**, 115267.
18 Z. Yu, H. Gong, F. Xue, Y. Zeng, X. Liu and D. Tang, *Anal. Chem.*, 2022, **94**, 13233–13242.
19 J. Shu and D. Tang, *Anal. Chem.*, 2020, **92**, 363–377.
20 R. Zeng, Z. Luo, L. Zhang and D. Tang, *Anal. Chem.*, 2018, **90**, 12299–12306.
21 R. Zeng, W. Wang, G. Cai, Z. Huang, J. Tao, D. Tang and C. Zhu, *Nano Energy*, 2020, **74**, 104931.
22 B. Jiang and M. Liang, *Chin. J. Chem.*, 2021, **39**, 174–180.
23 Z. Ding, M. Gao, C. Chen, P. Ni, C. Zhang, B. Wang, G. Duan and Y. Lu, *Chin. J. Chem.*, 2021, **39**, 3369–3374.
24 H. Wei and E. Wang, *Chem. Soc. Rev.*, 2013, **42**, 6060–6093.
25 L. Yang, X. Guo, Q. Zheng, Y. Zhang, L. Yao, Q. Xu, J. Chen, S. He and W. Chen, *Sens. Actuators, B*, 2023, **393**, 134165.
26 A. Scarsi, D. Pedone and P. Pompa, *Nanoscale Adv.*, 2023, **5**, 2167–2174.
27 F. Li, J. Jiang, H. Peng, C. Li, B. Li and J. He, *Sens. Actuators, B*, 2022, **369**, 132334.
28 L. Peng, C. Lin, L. Shi and F. Cai, *New J. Chem.*, 2021, **45**, 21538–21542.
29 Z. Yu, G. Cai, X. Liu and D. Tang, *ACS Appl. Mater. Interfaces*, 2020, **12**, 40133–40140.
30 Z. Gao, S. Lv, M. Xu and D. Tang, *Analyst*, 2017, **142**, 911–917.
31 Z. Gao, M. Xu, L. Hou, G. Chen and D. Tang, *Anal. Chim. Acta*, 2013, **776**, 79–86.
32 Y. Zheng, J. Wang, G. Chen, M. Wang, T. Chen, Q. Ke, Y. Huang, F. Cai, R. Huang and C. Fan, *Analyst*, 2022, **147**, 1923–1930.
33 W. Zhuang, Y. Li, X. Weng, H. Guo, Y. Zhang, Y. Yang and C. Fan, *Anal. Methods*, 2019, **11**, 1631–1638.
34 Z. Hong, G. Chen, S. Yu, R. Huang and C. Fan, *Anal. Methods*, 2018, **10**, 5364–5371.

© 2023 The Author(s). Published by the Royal Society of Chemistry